When Polymorphism in Metal-Organic Frameworks Enables Water Sorption Profile Tunability for Enhancing Heat Allocation and Water Harvesting Performance

Tobie Matemb Ma Ntep, Mohammad Wahiduzzaman, Eric Laurenz, Ieuan Cornu, Georges Mouchaham, Iurii Dovgaliuk, Shyamapada Nandi, Klaus Knop, Christian Jansen, Farid Nouar, et al.

When Polymorphism in Metal-Organic Frameworks Enables Water Sorption Profile Tunability for Enhancing Heat Allocation and Water Harvesting Performance

Tobie J. Matemb Ma Ntep, Mohammad Wahiduzzaman, Eric Laurenz, Ieuan Cornu, Georges Mouchaham,* Iurii Dovgaliuk, Shyamapada Nandi, Klaus Knop, Christian Jansen, Farid Nouar, Pierre Florian, Gerrit Füldner, Guillaume Maurin,* Christoph Janiak,* and Christian Serre*

M. Wahiduzzaman, E. Laurenz, and I. Cornu contributed equally to this work.

Affiliations

T. J. Matemb Ma Ntep, G. Mouchaham, I. Dovgaliuk, S. Nandi, F. Nouar, C. Serre;
Email: georges.mouchaham@ens.psl.eu; christian.serre@ens.psl.eu

1 Institut des Matériaux Poreux de Paris, Ecole Normale Supérieure, ESPCI Paris, CNRS, PSL University, 75005, Paris, France

T. J. Matemb Ma Ntep, C. Jansen, C. Janiak;
Email: janiak@uni-duesseldorf.de

2 Institut für Anorganische Chemie und Strukturchemie, Heinrich-Heine-Universität Düsseldorf, Universitätstraße 1, D-40225 Düsseldorf, Germany

M. Wahiduzzaman, G. Maurin
3 ICGM, Univ. Montpellier, CNRS, ENSCM, 34293 Montpellier, France
Email: guillaume.maurin1@umontpellier.fr

E. Laurenz, G. Füldner
4 Department of Heating and Cooling Technologies, Fraunhofer Institute for Solar Energy Systems ISE,Heidenhofstr. 2, 79110 Freiburg, Germany

I. Cornu, P. Florian
5 Centre National de la Recherche Scientifique (CNRS), UPR3079 CEMHTI, Université d'Orléans, 1D Av. Recherche Scientifique, CEDEX 2, 45071 Orléans, France

K. Knop

6 Institut für Pharmazeutische Technologie und Biopharmazie, Heinrich-Heine-Universität Düsseldorf, Universitätstraße 1, D-40225 Düsseldorf, Germany

Keywords: Metal-Organic Frameworks, polymorphism, hydrophilicity, water sorption, adsorption-driven cooling, water harvesting.

Abstract

The development of thermally driven water-sorption-based technologies relies on high-performing water vapor adsorbents. Here, polymorphism in Al-metal-organic frameworks is disclosed as a new strategy to tune the hydrophilicity of MOFs. This involves the formation of MOFs built from chains of either *trans*- or *cis*- μ-OH-connected corner-sharing $AlO_4(OH)_2$ octahedra. Specifically, [Al(OH)(muc)] or MIP-211, is made of *trans*, *trans*-muconate linkers and *cis*-μ-OH-connected corner-sharing $AlO_4(OH)_2$ octahedra giving a 3D network with sinusoidal channels. The polymorph MIL-53-muc had a tiny change in the chain structure that results in a shift of the step position of the water isotherm from P/P_0 ~ 0.5 in MIL-53-muc, to P/P_0 ~ 0.3 in MIP-211. Solid-state NMR and Grand Canonical Monte Carlo revealed that the adsorption occurs initially between two hydroxyl groups of the chains, favored by the *cis*-positioning in MIP-211, resulting in a more hydrophilic behavior. Finally, theoretical evaluations showed that MIP-211 would allow achieving a coefficient of performance for cooling (COPc) of 0.63 with an ultralow driving temperature of 60 °C, outperforming benchmarks sorbents for small temperature lifts. Combined with its high stability, easy regeneration, huge water uptake capacity, green synthesis, MIP-211 is among the best adsorbents for adsorption-driven air conditioning and water harvesting from the air.

1. Introduction

The development of many sustainable technologies involving the adsorption of water vapor strongly relies on the discovery of high-performing porous materials. Such technologies include adsorption-driven heat transformation (AHT) and atmospheric water harvesting (AWH).[1,2,3,4,5,6] In water-based adsorption-driven heat exchangers, that is adsorption-driven chillers (ADCs) and adsorption heat pumps (AHPs), heating or cooling, e.g., for air-conditioning, are achieved by reversible multicycling adsorption-desorption of water vapor into/from a porous adsorbent. The regeneration of the material at each cycle could be realized by applying a (low temperature) renewable energy, such as solar or waste heat (see the working principle in the supporting Figure S1).[7,8] ADCs and AHPs are regarded as a clean and sustainable alternative to compressor-based conventional chillers and heat pumps, on account of their potential to minimize primary electrical energy consumption and greenhouse gas emissions generated by industrial or domestic cooling.[9,10,11] On the other hand, AWH enables to capture water vapor directly from thin air by porous materials during relatively high humidity times, e.g., at night, and to release the trapped water upon solar heating during daytime (see the principle in supporting Figure S2).[12,13,14] AWH represents, therefore, an attractive means for the delivery of drinking/fresh water in remote and arid areas.[15,16] For both technologies, the applied porous material should, among other criteria, adsorb water vapor at low relative humidity (5% ≤ RH ≤ 40%) and release it with a minimal energy penalty. To meet a good performance/efficiency of the device, water adsorption onto the porous material should also occur within a very narrow relative pressure window, which is translated by a single-step sigmoidal (S-shaped) water isotherm, as well as a high uptake capacity should be reached within the pressure window of interest.[17,18,19]

Among several types of porous adsorbents that have already been investigated for both AHT and AWH, metal-organic frameworks (MOFs) are appealing materials.[20,21,22,23,24] This is due to the wide range of possibilities that this materials class can offer in terms of tuning their water sorption profile, as well as large water uptake capacities attainable due to their high porosity.[25,26,27,28,29] MOFs consist of inorganic building units (IBUs; i.e., clusters, chains or layers) that are interconnected by polydendate organic linkers to form a micro- or meso-porous coordination network.[30,31,32] Unlike more traditional porous materials like zeolites and activated carbons, the combination of several parameters such as ligands or clusters functionalization, framework topology, pore geometries and size, the presence of structural defects etc., allow modulating the water sorption profile of MOFs in a unique manner.[33,34,35,36,37] Several of these strategies to design MOFs for water-based applications have been implemented in order to increase their hydrophilicity, their water uptake capacity, their hydrothermal stability or to yield a water isotherm with a steep sigmoidal shape.[38,39,40,41,42] Regarding tuning the pore size and/or shape of MOFs, polymorphism could

be a new approach to modulate the water sorption properties of a MOF while maintaining its building blocks. Polymorphism means the occurrence of a compound in diverse crystalline structures possessing the same chemical composition (stoichiometry), but differ in the spatial arrangement of the atoms which leads to variation in physicochemical properties. MOF polymorphs are also referred to as framework isomers.[43,44,45,46,47] The significance of polymorphism of MOFs has been recognized, since one topological isomer can exhibit different or enhanced properties compared to the other.[48,49,50] For instance, two polymorphs of MOF Tl^{I}(TCNQ) (TCNQ = 7,7,8,8-tetracyanoquinodimethane), which crystallize in the space groups $P2_1/c$ and $P2/c$, respectively, displayed dramatically different conductivity properties.[51] The **nbo** topology of Cu_2(1,4-benzenedicarboxylate) was reported to feature a remarkably high affinity for linear alkanes due to its small pores, unlike its polymorphs with **rhr** and **lvt** topologies, respectively.[52] However, this approach has not yet been addressed, to the best of our knowledge, for improving MOFs for water adsorption and related applications.

Aluminum-based MOFs (Al-MOFs) are particularly attractive for cycling water-adsorption applications on account of their hydrothermal and chemical stabilities, as well as their light specific weight, the non-toxicity and low-cost of aluminum.[53,54] Many structurally similar Al-MOFs which are built from chains of μ-OH and carboxylate bridged {AlO_6} octahedra shared vertices through the μ-OH bridge and have been well studied for their potential in AHT and AWH applications, including MIL-53-Fum,[55,56] CAU-10H,[57,58,59,60] MIL-53-TDC,[61] CAU-23,[62] MOF-303,[63] MIL-160,[64,65,66], KMF-1,[67] and CAU-10pydc.[68] Interestingly, these MOFs share the same general unit formula ([Al(OH)(L)]; where L= dicarboxylate linker) but can differ in the shape of the Al-O chain, and the corresponding geometrical features (such as the pores shape and dimension).[69] In general, using ditopic linear linkers yields Al-MOF structures with chains of *trans*-μ-OH-connected (or *trans*-connected) corner-sharing AlO_6 octahedra (e.g., MIL-53 topology),[70,71] while using “V-shaped” linkers yields Al-MOFs with helical chains of *cis*-μ-OH-connected (or *cis*-connected) corner-sharing AlO_6 octahedra (e.g., CAU-10 topology).[72,73] Exceptions to this general observation are V-shaped 1H-pyrazole-3,5-dicarboxylate and 2,4-furandicarboxylate that yield chains of alternate *cis*-connected and *trans*-connected corner-sharing AlO_6 octahedra in MOF-303 and MOF-333, respectively.[74] Likewise, V-shaped 2,5-thiophenedicarboxylate yields polymorphs of either rod-like chains in MIL-53-TDC or chains of mixed *cis*/*trans* corner-sharing AlO_6 octahedra in CAU-23.[62] The trend which emerges from previously reported works on Al-MOFs, shows that dicarboxylates with opening angle, defined by the axes of C-C bonds of the carboxylate groups, whose values are strictly over 150-158° yield chains of *trans*-connected corner-sharing AlO_6 octahedra, while those strictly below 150° yield chains of *cis*-connected corner-sharing AlO_6 octahedra. An opening angle of about 150-158° seems to be an inflection point, and

therefore results in Al-MOFs either with chains of mixed *cis*/*trans*-connected corner sharing AlO_6 octahedra (CAU-23) or chains of alternate *cis*-connected and *trans*-connected corner-sharing AlO_6 octahedra (MOF-303, MOF-333 and MIL-53-TDC, respectively) (see Scheme 1 and Figure S3).[75] Until now, to the best of our knowledge, no linear dicarboxylate-based linker has yet been reported to yield an Al-MOF containing helical Al-O chain clusters. Yet, just as with V-shaped linkers, polymorphism through rod-like or helical chains should be conceivable also with linear linkers in Al-MOFs. This offers a new opportunity to tune the pore shape and framework topology of already established Al-MOFs. In this regard, the use of flexible ligands (i.e., with aliphatic core, saturated or not) could be a rational strategy.

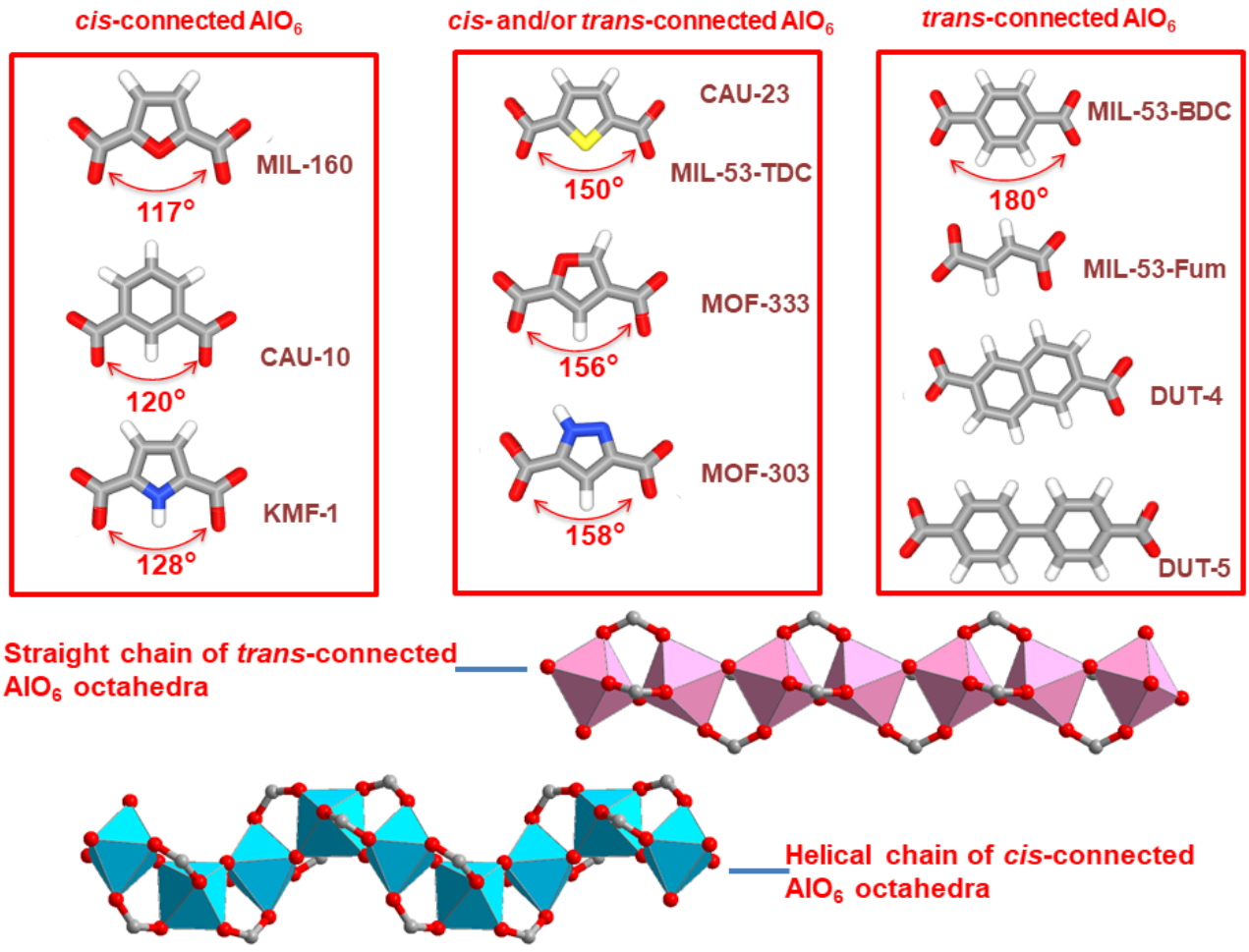

Scheme 1. Structures and opening angles of some dicarboxylate linkers that have been used to construct Al-MOFs made up of Al-O chains. Linkers that yield Al-MOFs made up of helical Al-O chains (left), linkers that yield Al-MOFs made up of mixed helical and/or straight Al-O chains (middle), and linkers that yield Al-MOFs made up of straight Al-O chains (right). Shared corners of AlO_6 octahedra are bridging μ-OH groups, which are *trans*-positioned or *cis*-positioned in straight or helical chains, respectively. Opening angles of V-shaped dicarboxylates were measured from their structure from cif files (CSD-Refcodes: MIL-160, PICBAH; CAU-10, CELZUQ; KMF-1, KUZPUT; CAU-23, ZOVHUQ; MOF-303, CAMTET; MOF-333, CAMYEY).

In the case of the zigzag-spaced, pseudo-linear *trans,trans*-muconate linker (from *trans*,*trans*-1,3-butadiene-1,4-dicarboxylate = muc^{2-}), some of us recently obtained, using this linker, a new Al-MOF, MIL-53-muc,[76] showing MIL-53's topology similarly to the aluminum

fumarate MOF (MIL-53-Fum),[77] where its framework is made up of rod-like chains of *trans*-μ-OH-corner-sharing AlO_6 octahedra. This was expected since muconate can be regarded as a twofold extension of the fumarate linker. The water sorption profile of MIL-53-muc displays an S-shaped isotherm like MIL-53-Fum, but with a higher uptake capacity and the step position shifted to higher relative pressures (P/P_0 = 0.5–0.6), compared with that of MIL-53-Fum whose step is found at a relative pressure of P/P_0 = 0.2–0.3.[76] This is in line with an increase in hydrophobic behavior, rationally attributed to the extension of the hydrophobic organic chain in the muconate linker and lower confinement effect due to larger channels. Hence, the resultant water sorption profile of MIL-53-muc renders this MOF unsuitable for AHT applications when paired with water as cooling fluid, since the step position of the isotherm is located beyond P/P_0 = 0.4.

Herein, we disclose polymorphism in aluminum muconate MOFs which consists of a simple twisting of the linear chain of *trans*-μ-OH-connected corner-sharing AlO_6 octahedra into a helical chain of *cis*-μ-OH-connected corner-sharing AlO_6 octahedra (Figure 2). Remarkably, without any significant difference in pore size/shape and volume, such a subtle structural modification results, however, in a drastic change in the water sorption profile, as it switches the inflection point (α) — i.e., the relative pressure at which half of the total adsorption capacity is reached — of the less hydrophilic aluminum muconate phase MIL-53-muc from α = 0.54 to α = 0.29 in the (much) more hydrophilic new phase MIP-211. In-depth investigations combining Density Functional Theory (DFT) and *in situ* solid-state NMR (ssNMR) along with Grand Canonical Monte Carlo (GCMC) simulations were carried out to study the water sorption mechanism in both aluminum muconate MOFs, and thus, to understand the origin of this remarkable difference. MIP-211 was then assessed as a potential adsorbent material applicable for adsorption cooling due to its S-shaped water vapor isotherm with a steep uptake at a relative pressure of P/P_0 = 0.26–0.3, a high uptake capacity of 0.50 $g_{H2O}\, g_{MOF}^{-1}$ at this relative pressure and excellent stability upon cycling.

2. Results and discussion

2.1. MOF Synthesis

The newly obtained aluminum muconate, MOF MIP-211, was initially synthesized from the reaction of *t,t*-muconic acid (H_2muc) with aluminum sulfate octadecahydrate [$Al_2(SO_4)_3{\cdot}18H_2O$] in a water/DMF (3/1) mixture (DMF = *N*,*N*′-dimethylformamide) under reflux conditions. The solvothermal treatment (T = 120 °C) of similar reaction mixture lead to the formation of a crust-like unidentified crystalline material (see powder X-ray diffraction, PXRD, pattern in Figure S5) The reported aluminum muconate phase MIL-53-muc was

instead obtained from the reaction of H_2muc with aluminum nitrate hexahydrate [$Al(NO_3)_3 \cdot 6H_2O$] in a water/DMF mixture under solvothermal conditions (see synthesis details in the experimental section).[76] The reflux treatment of a similar mixture leads to the formation of the phase of MIL-53-muc still, albeit with poor crystallinity (see PXRD pattern in Figure S5). The comparison of PXRD patterns of MIP-211 and MIL-53-muc (Figure 1a and Figure S4) gave the first indication of the structural difference between the two materials. The formula of dehydrated MIP-211 suggested from CHN elemental analysis (see supporting information) is shown to be [Al(OH)(muc)], as in the case of MIL-53-muc. This suggested that MIP-211 and MIL-53-muc are aluminum muconate polymorphs. The modeled structure and the Rietveld refinement of data from high-resolution PXRD data for MIP-211 (Figure 1b) confirmed this hypothesis. Furthermore, analyses of the NMR parameters calculated by DFT calculations and obtained from solid-state NMR (ssNMR) measurements were found to be in agreement with this hypothesis, as MIP-211 and MIL-53-muc featured very similar ^{1}H MAS spectra and ^{13}C CP MAS spectra (Figures 1d, e, and S37 & S38) attesting that the linker has very similar configurations in both MOFs. One could nevertheless note a narrower ^{13}C line width for MIP-211 (see spectra simulation in Figure S6 and resulting parameters in Tables S1 & S11), pointing to a slightly more ordered structure. MIL-53-muc ^{1}H lines were, however, narrower than for the MIP-211 ones (Figure S7 and Table S2) but only for the most shielded ^{1}H peak at 2.1 ppm, ascribed to the bridging μ-OH of the chain based both on its position,[78] and on the ^{27}Al{^{1}H} correlation experiments (Figure S8). This broadening observed for this μ-OH peak in ssNMR in MIP-211 may reveal a dynamic behavior in interaction (possibly exchanging) with a small amount of residual water in the pores. MIP-211 and MIL-53-muc displayed also very similar infrared and Raman spectra (Figure S15 and S16), with a band at about 3600 cm^{-1} ascribed to μ-OH, which also corroborates closely related polymorphs. Besides, scanning electron microscopy (SEM) showed rectangular prismatic microcrystals of ~0.3 µm wide and ~0.5-2 µm long for MIL-53-muc, against elongated rectangular bipyramid microcrystals of ~2.5 µm wide and ~8.5 µm long for MIP-211 (Figure S17).

MIP-211 exhibits a type I nitrogen-adsorption isotherm at 77 K (Figure 1c) associated with a BET surface area of 1450 $m^2\ g^{-1}$ and pore volume of 0.60 $cm^3\ g^{-1}$. This is close to the values of MIL-53-muc whose BET area and pore volume are 1500 $m^2\ g^{-1}$ and 0.63 $cm^3\ g^{-1}$, respectively. Theoretical surface areas (2140 $m^2\ g^{-1}$ and 2200 $m^2\ g^{-1}$) and free pore volumes (0.86 $cm^3\ g^{-1}$ and 0.85 $cm^3\ g^{-1}$) calculated from the DFT optimized crystal structures of MIP-211 and MIL-53-muc solids, respectively, also confirm that both solid possess nearly identical porosities although values are slightly higher than the experimental ones most likely assigned to the presence of remaining solvent in the pores.

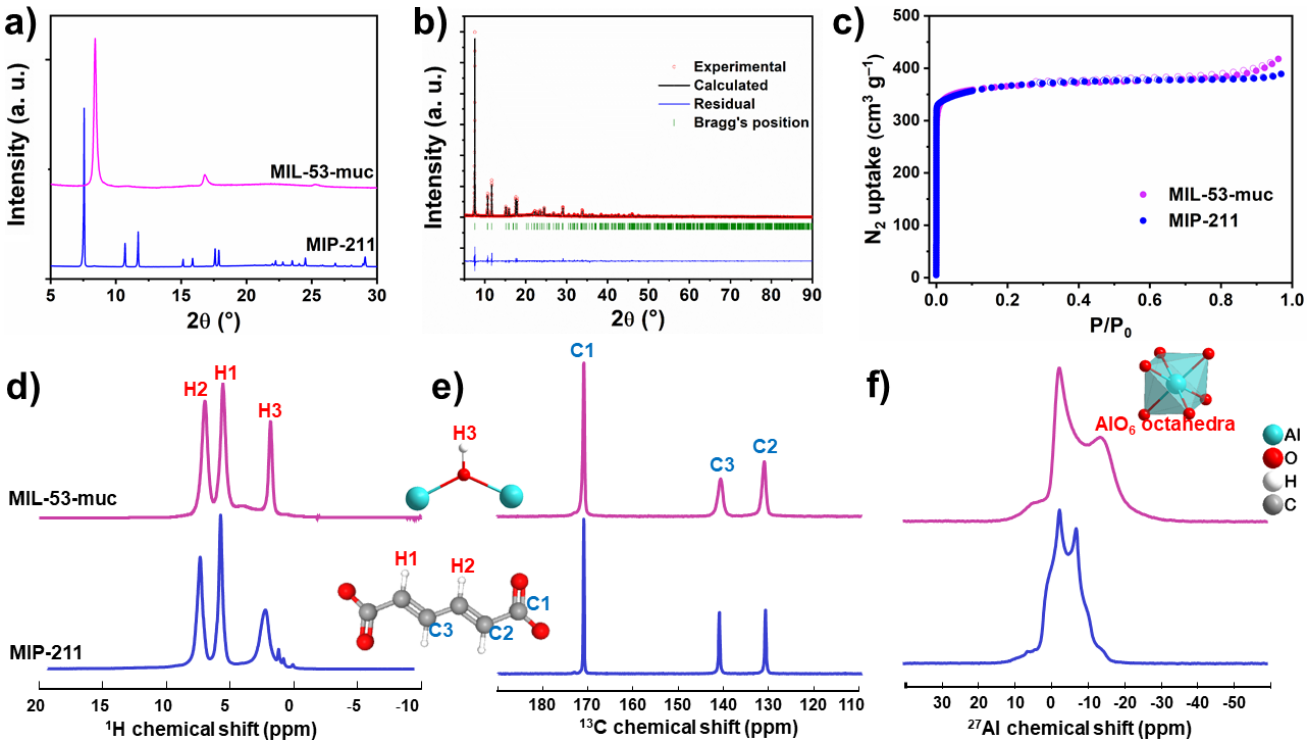

Figure 1. PXRD patterns under Cu-Kα radiation (λ = 1.5418 Å) of MIP-211 and MIL-53-muc (a), final Rietveld plot for hydrated MIP-211 (b), nitrogen sorption isotherms at 77 K (adsorption and desorption branches are represented by full and empty symbols, respectively) (c). ^{1}H (d), ^{13}C (e), and ^{27}Al (f) CPMAS ssNMR spectra of MIP-211 and MIL-53-muc.

2.2. Structural aspects

The structure of MIP-211 was solved using the direct space method in FOX,[79] and then refined by the Rietveld method from high-resolution powder X-ray diffraction (HR-PXRD) data using Fullprof (see more details in the supporting information).[80] The dried and hydrated MIP-211 crystallizes in the tetragonal centrosymmetric space group $I4_1/acd$, with similar unit cell parameters of $a = b = 23.4208(3)$ Å and $c = 10.9733(3)$ Å (dried form), and $a = b = 23.4148(3)$ Å and $c = 10.9510(3)$ (hydrated form) (see Tables S4-S6), in agreement with a rigid character of this framework. DFT optimization performed on the dried form of this solid shows that the most energetically favorable crystal structure is associated with a slightly expanded unit cell volume (<4.0 %) as compared to the experimental one (see Table S10). A close inspection of the crystal structure of MIP-211 reveals that it is made up of helical chains of *cis*-connected corner-sharing AlO_6 octahedra, as observed for CAU-10H and MIL-160.[81] However, neighboring chains in MIP-211 are translation images of each other, unlike MIL-160 where neighboring chains are mirror images of each other (Figure S21). The chains in MIP-211 are bridged by *t,t*-muconate linkers (muc), whereby each carboxylate group of the muc linker connects two Al centers from the same chain in a bidentate bridging (μ- κ^2O:O' mode) fashion. This leads to a three-dimensional network forming one-dimensional

sinusoidal channels with a square-shaped cross-section of ~8.5 × 8.5 Å^2 (Figure 2 and Figures S22 & S36). MIP-211 can therefore be regarded as a polymorph of MIL-53-muc resulting from screw-twisting the straight Al-O chains of *trans*-corner-sharing AlO_6 octahedra in the structure of MIL-53-muc, all other elements being equal (Figure 2 and Figure S22 & S23). So far, to our knowledge, such a polymorphism hasn't been reported for MOFs with the same ligand. This can be accounted to the degree of flexibility that muc ligand allows. Indeed, a close comparison between the ligands in the two MOF structures reveals, as shown in Figure S24, some conformational differences needed for their accommodation within each of the frameworks.

The ^{27}Al spectra (Figure 1f) displayed a single well-defined quadrupolar-like component for MIP-211, while a more complex line shape is found for MIL-53-muc associated with a distribution of environments. ^{27}Al MQMAS experiments (Figure S9) confirmed this analysis with the presence of at least a second component for MIL-53-muc. DFT calculated ^{27}Al NMR parameters and corresponding NMR spectra reported in supporting information Table S12, and Figures S37c, S38c are in very good agreement for MIP-211 with a predicted single Al site with quadrupolar coupling constant (C_Q) of 4.93 MHz and asymmetry parameter η_Q of 0.53 in excellent agreement with the corresponding experimental values of 5.1 MHz and 0.48, respectively. Regarding MIL-53-muc, the DFT calculations reveal two almost equivalent Al associated with very similar C_Q (8.04 MHz and 7.93 MHz) and η_Q (0.18 and 0.19) that match with the values experimentally obtained for one Al site (8.7 MHz and 0.18), however they do not support the existence of the second Al site (C_Q= 5.1 MHz and η_Q=0.11) with the consideration of the optimized structure of MIL-53-muc in its open form. This deviation could therefore be ascribed to a slight breathing effect of the structure (common in MIL-53-type MOFs) creating different local environment for Al sites (the sample can show different phases depending on the pore filling and/or opening angles). The NMR parameters retrieved from the simulations of the experimental NMR spectra (Figure S10 and Table S3) and the DFT calculations (Table S12, and Figures S37c & S38c) showed marked differences between the two MOFs corroborating that the structural dissimilarities between MIP-211 and MIL-53-muc stem primarily from the connection linking the AlO_6 octahedra (*cis*-connected vs *trans*-connected) and therefore the shape of the resulting Al-O chains.

Interestingly, MIP-211 is to the best of our knowledge, the first reported Al-MOF made up of helical Al-O chains which incorporate a linear linker. This suggests that analogous polymorphs of MIL-53-type Al-MOFs with linear linkers like terephthalate and fumarate could be conceivable.

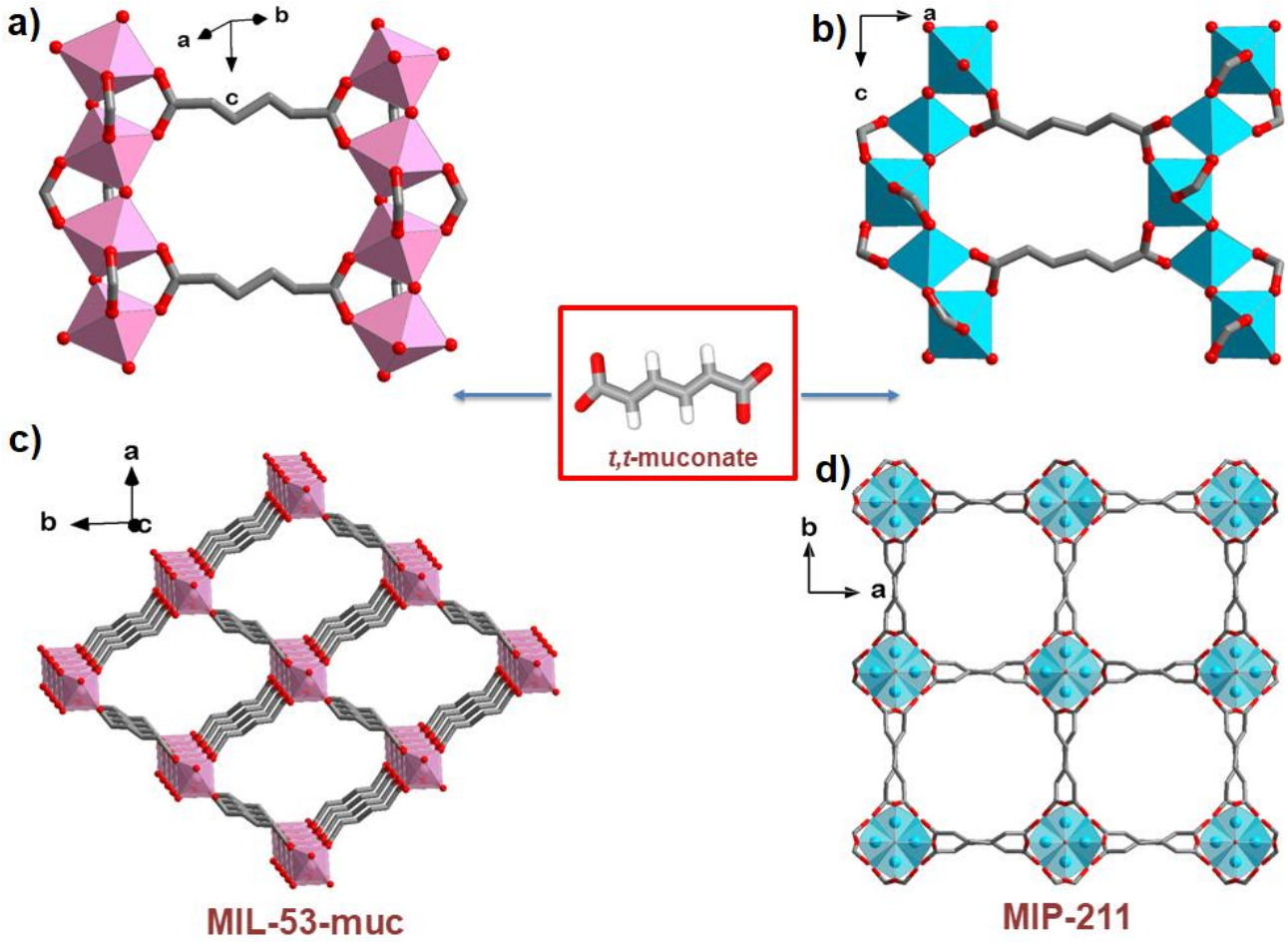

Figure 2. Comparative structures of MIL-53-muc (left) and MIP-211 (right), showing *t*,*t*-muconate linkers bridging two straight Al-O chains in MIL-53-muc (a) and two helical Al-O chains in MIP-211 (b). The projection along the [001] direction disclosing the one-dimensional channels with lozenge-shaped cross-section in MIL-53-muc (c) and square-shaped cross-section in MIP-211 (d). Al, pink and blue polyhedral in MIL-53-muc and MIP-211, respectively; C, gray; O, red. Water molecules and hydrogen atoms are omitted for clarity.

2.3. Water sorption profile

The investigation of their water vapor sorption behavior showed that MIL-53-muc displays a single-step sigmoidal (S-shaped) water sorption isotherm with the large step located at the relative pressure P/P_0 = 0.5–0.6 and a moderate hysteresis loop between the adsorption and desorption branches (Figure 3a). A step located above P/P_0 = 0.4 indicates that MIL-53-muc can be regarded as a more hydrophobic material,[8,33,55] and could have a slight water-induced network flexibility as often observed for MOFs with the MIL-53 topology.[82] At 25 °C, The water uptake capacity of 0.50 g_{H2O} g^{-1}_{MOF} at P/P_0 = 0.6 slightly increases to 0.60 g_{H2O} g^{-1}_{MOF} at P/P_0 = 0.9. Unlike MIL-53-muc, MIP-211 features an S-shaped water vapor isotherm with no hysteresis loop between the adsorption and desorption branches, which confirms the rigidity of MIP-211's framework. At 25 °C, the adsorbed amount of water increases gradually with increasing relative pressure up to 0.10 g_{H2O} g_{MOF}^{-1}, right below P/P_0 = 0.3, which is followed by a steep uptake to 0.50 g_{H2O} g_{MOF}^{-1} at about P/P_0 = 0.3, and eventually reaches 0.60 g_{H2O} g_{MOF}^{-1} at P/P_0 = 0.9 (Figure 3a). Interestingly, the step position in the water isotherm of MIP-211 is drastically shifted to a lower relative pressure of about P/P_0 = 0.3,

compared with that of MIL-53-muc, meanwhile the water uptake capacity both at the step position and the total water capacity remains almost unchanged in agreement with their similar pore volumes. The step position of the water isotherm at P/P_0 = 0.3 makes MIP-211 a comparatively far more hydrophilic solid. This shift was unexpected since the two MOFs are both made up of the same muconate linker and AlO-chains with bridging μ-OH-groups having only a different configuration. Moreover, both frameworks feature similar pore geometries (lozenge- vs square-shaped 1D channels, Figure 2c, d), and essentially identical surface areas and pore volumes (*vide supra*). Therefore, at first sight, one would expect both MOFs to also feature similar water affinity. Remarkably, the polymorphism between MIL-53-muc and MIP-211, which consists of twisting the straight linear Al-O chains into helical Al-O chains, appears to be a strategy to tune the hydrophilicity or in general the guest affinity to MOFs.

It is worth mentioning that, among the benchmark Al-MOFs already investigated for water-adsorption-based applications, the water sorption isotherm of MIP-211 is particularly close to that of CAU-23 in terms of the inflection points position (α =0.27 and 0.29 at 25 °C; Figure 3e), the steepness of the uptake step (almost vertical for both MOFs), the insignificant hysteresis loop, and the enthalpy of water adsorption (ΔH_{ads} = -48.2, and -48.5 kJ mol^{-1} for CAU-23,[62] and MIP-211, respectively; vide infra). However, the IBU (Inorganic Building-Unit) in CAU-23 consists of chains of mixed *cis*- and *trans*-μ-OH-connected AlO_6 octahedra, unlike chains of exclusively *cis*-μ-OH-connected AlO_6 octahedra in MIP-211, the latter having also a far higher water uptake and working capacity (around the step) compared with CAU-23. Meanwhile, one should also highlight the polymorph of CAU-23, namely MIL-53-TDC, consisting of chains of exclusively *trans*-μ-OH-connected AlO_6 octahedra, that features slightly lower hydrophilicity, manifested by the large water uptake step located at a relative pressure slightly over P/P_0 = 0.3 (Figure S25). The minor shift of the inflection point at 25 °C from α = 0.35 in MIL-53-TDC to α = 0.29 = CAU-23, which was not previously emphasized, is likely due to the partial presence of *cis*-connected AlO_6 octahedra in the framework of CAU-23. Consequently, unlike MIP-211 the sole presence of only *cis*-μ-OH-connected AlO_6 octahedra can be seen as a way to induce a drastic shift of the water isotherm step towards lower relative pressures, with respect to MIL-53-muc (only *trans*-μ-OH). This comparison establishes the polymorphism of *trans*-connected *vs cis*-connected AlO_6 octahedra as a new approach to significantly tune (increase) the hydrophilicity (or to adjust the position of the water pressure step) of Al-MOFs.

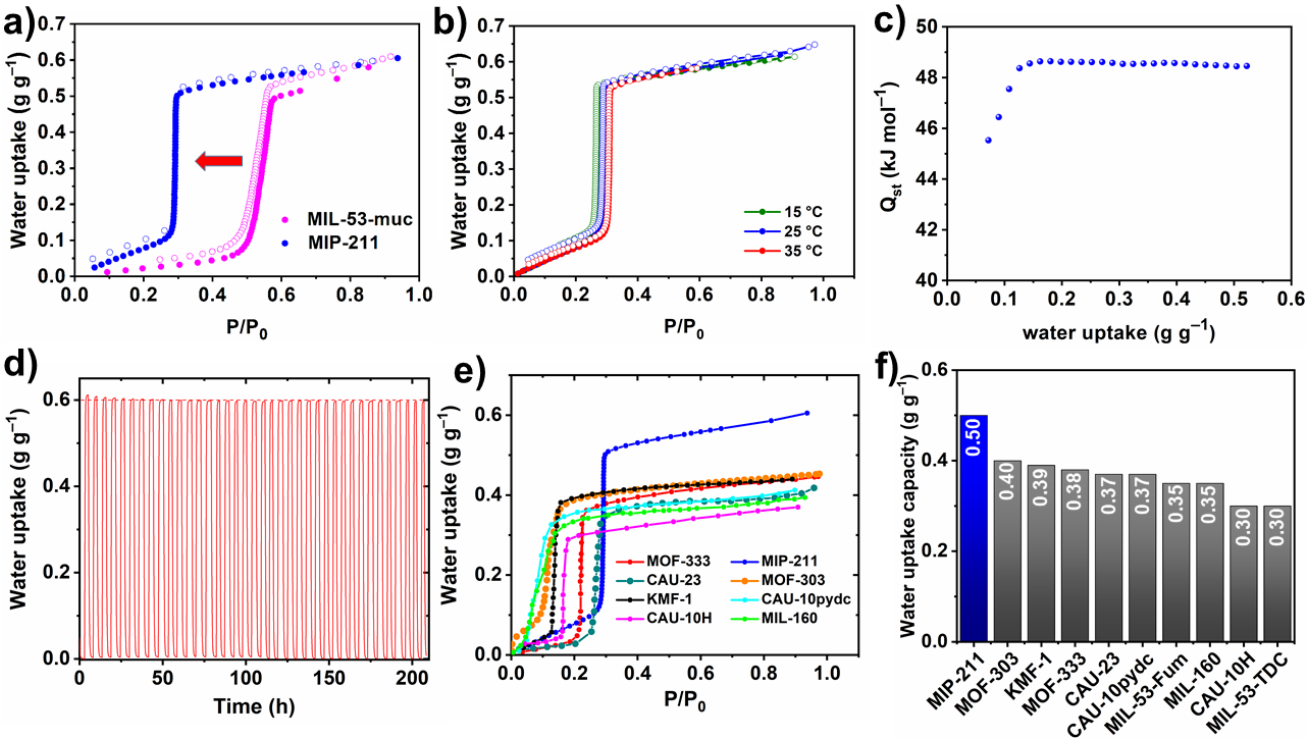

Figure 3. a) Water sorption isotherms of MIP-211 (blue) and MIL-53-muc (magenta) at 25 °C. b) Water sorption isotherms of MIP-211 at 15 °C, 25 °C and 35 °C. c) Plot of isosteric heat of water adsorption for MIP-211. d) Multicycling stability test of MIP-211 showing the water uptake during 40 full adsorption-desorption cycles. e) Water adsorption isotherms of MIP-211 and some benchmark Al-MOFs at 25 °C (data were collected from ref.[34], MIL-160; ref.[57], CAU-10H; ref.[62], CAU-23; ref.[63], MIL-53-Fum; ref.[67], KMF-1; ref.[68], CAU-10pydc; ref.[74], MOF-303 and MOF-333). f) Comparison of the water uptake capacity of MIP-211 with other high-uptake capacity of metal carboxylate MOFs at P/P$_0$ = 0.3 and 25 °C. Adsorption and desorption isotherms are represented by full and empty symbols, respectively.

2.4. Probing the crystal structure-water sorption relationship by ssNMR

To get more insights on the interactions between water and the MOF frameworks, we have deployed advanced ssNMR studies. Upon hydration, the ^{13}C signals appeared not affected whereas ^{1}H peaks shift and ^{27}Al lines broaden (see Figure S11), which is related to the increase of pore volume when filled with water. For both MOFs, the peak related to water dominates the ^{1}H spectra at around 4 ppm, the peak related to µ-OH environments at 2.1 ppm disappears and that related to the muconate slightly shifts (approx. 0.2 ppm) without changing line widths. This is better seen upon hydration with D_2O which reduces considerably the water peak (Figure S12) with at least two water components and a small peak near 5 ppm. The former are assigned to the H_2O molecules in contact with the pore walls and inside the pores,[34] while the later peak is undoubtedly assigned to µ-OH environments based, again, on ^{27}Al{^{1}H} double resonance D-HMQC (dipolar heteronuclear multiple-quantum coherence) experiments which dramatically increases its intensity (Figures S8 and S12). In the case of MIL-53-muc, this µ-OH peak is found at 4.6 ppm with a width of 0.84 ppm whereas for MIP-211 its maximum is at 5.1 ppm with a width of 0.37 ppm (see

Figure S13 and Table S2). The strong positive shift seen for both compounds indicates a strong μ-OH / H_2O chemical interaction, and the bigger line width for MIL-53-muc than MIP-211 suggests a stronger interaction for the former. This is the opposite behavior with respect to the dried sample (see Figure S12), suggesting that the degree of hydration may play a significant role in the μ-OH / water interaction. In all cases, the hydrophilic character seems to be controlled by the μ-OH sites.

Furthermore, the resolution provided by the hydration with D_2O was exploited to measure the water self-diffusion coefficient using ^1H pulse-field gradient (PFG) NMR under magic angle spinning (Figure S14). For both compounds, the main component at 4.0 ppm diffuses faster (D_S = 1.82 10^{-9} m^2/s for MIL-53-muc and D_S = 1.41 10^{-9} m^2/s for MIP-211) and is related to bulk water not interacting with the pore walls, but, as expected, diffusing slower than in bulk water at room temperature (D = 2.01 10^{-9} m^2/s).[83] Additional components at 4.3 ppm and 3.7 ppm for MIL-53-muc exhibit D_S = 1.34 10^{-9} m^2/s and 1.47 10^{-9} m^2/s, respectively, whereas for MIP-211 a single additional component is found at 4.3 ppm with D_S = 1.12 10^{-9} m^2/s. The reduced self-diffusion coefficient confirms their attribution to water molecules in interaction with the pore walls. All types of water molecules are diffusing slower in MIP-211 than MIL-53-muc as a consequence of stronger interactions with the walls and in line with a lower hydrophobicity of this compound. The absolute values of D_S retrieved here are in line with those obtained in MIL-100(Fe),[84] but much higher than those of MIL-53(Cr) or MIL-100(Al).[85,86] This could be due to the fact that, to our best knowledge, for the first time, our PFG measurements are performed under MAS conditions, with deuterated water and at high magnetic field (17.6 T).

2.5. Molecular understanding of the water sorption mechanism

GCMC simulations were performed to shed light on the microscopic origin of the water adsorption performance of MIL-53-muc and MIP-211. As shown in Figure S39, the overall shape of the experimental water adsorption isotherms, particularly the positions of the step on the P/P_0 axis are well reproduced for both MOFs confirming the lower hydrophobicity of MIP-211 compared to MIL-53-muc. The slight overestimation of the total uptakes at saturation pressure is attributed to larger free pore volumes of the DFT optimized geometries compared to the experimental porosity determined from N_2 adsorption measurements (Table S10). Both MOFs possess very similar hydrophobic pore confinement (~8.5 Å in diameter, Figure S36). However, the density of the hydrophilic μ-OH sites is much higher ($r_{O(\mu 2OH)\text{-}O(\mu 2OH)}$ = 2.8 Å vs 3.75 Å) in the Al-O helical chain of MIP-211 solid compared to that in the Al-O rod of MIL-53-muc framework. As such, due to the strong dominance of the hydrophobic character of the confined pore geometry, the hydrophilic μ-OH sites of MIL-53-muc are able to adsorb water molecules only at a relative pressure, P/P_0 = 0.50 (Figure 4a). Upon increment of water vapor pressure, those water molecules anchored to the μ-OH (primary nucleation sites)

enable the adsorption of additional water molecules and form hydrogen bonds with other neighboring μ-OH sites of the pore walls (Figure 4b). The associated adsorption enthalpy calculated at the beginning of this water clustering process is quite low (~ -33 kJ/mol) in line with the hydrophobicity of MIL-53-muc. Notably, the radial distribution functions (RDFs) for H_2O/H_2O and H_2O/ μ-OH pairs calculated at this intermediate pore filling pressure (viz., P/P_0 = 0.60) indicate that although water molecules strongly interact with the μ-OH sites with a separating distance of 2.7 Å. Intermolecular water-water interactions supersede the former as evidenced by the relatively higher intensity of the corresponding RDF peak centered around 2.8 Å (Figures 4g). Further, an increase of the water vapor pressure to P/P_0 = 0.75 leads to a complete filling of MIL-53-muc porosity as depicted in Figure 4c.

In the case of MIP-211, at the beginning of the adsorption process at P/P_0 = 0.30, we note that a single water molecule effectively interacts with two μ-OH sites (Figure 4d) resulting in a simulated adsorption enthalpy of -45 kJ/mol, which is higher than the value obtained for MIL-53-muc and in line with its overall reduced dominance of the hydrophobic character. The RDFs presented in Figures 4h for the intermolecular $O(H_2O)…O(\mu\text{-}OH)$ interaction show a first peak at 2.8 Å accompanied by a wider shoulder spanning up to 3.2 Å, corroborating that these μ-OH sites are likely to attract water molecules much strongly as compared to MIL-53-muc. As shown in Figure 4e, a subtle increase of water vapor pressure from 0.30 to 0.35, over half of the MIP-211 porosity is filled with water molecules. These adsorbed water molecules form additional hydrogen bonds with other μ-OH sites in vertical (along the channel) and lateral directions facilitating a quick filling of the entire porosity at P/P_0 = 0.40 (see Figure 4f.

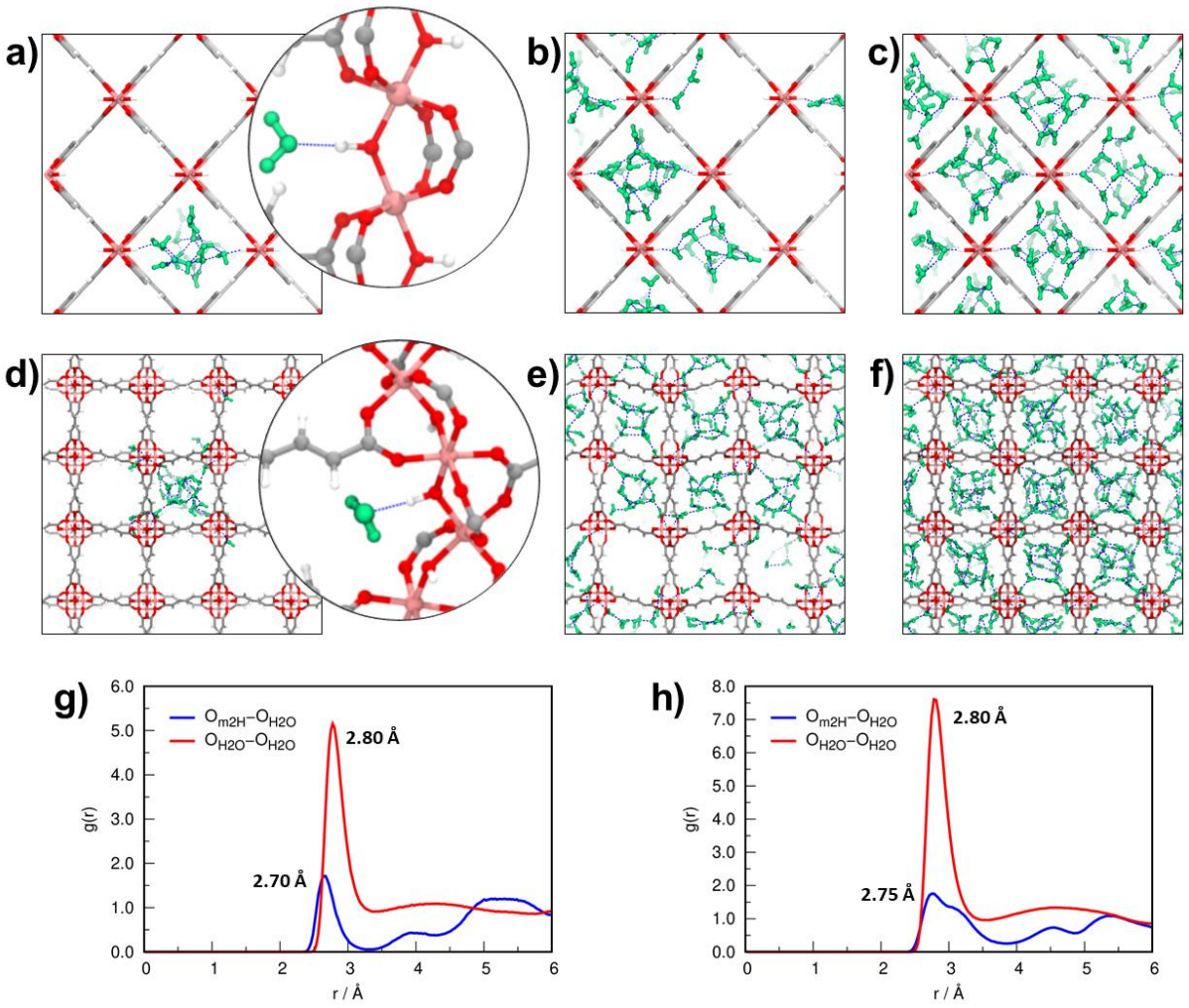

Figure 4. GCMC simulated adsorption mechanism of water for MIL-53-muc and MIP-211 MOFs at *T* = 298 K. Top panel: water adsorption snapshots for MIL-53-muc at P/P_0 = 0.50 (a), P/P_0 = 0.60 (b), and P/P_0 = 0.75 (c). Middle panel: water adsorption snapshot for MIP-211 at P/P_0 = 0.30 (d), P/P_0 = 0.35 (e), and P/P_0 = 0.40 (f). Subfigures (a) and (d) also show a close-up view of typical water interaction with μ-OH sites in MIL-53-muc and MIP-211, respectively. Atom color codes: O red; H white, C grey, Al pink, adsorbed water molecules are presented in green for easy distinction. Bottom panel shows the radial function distributions calculated for the water/water and water/ μ-OH pairs in MIL-53-muc at P/P_0 = 0.60 (g) and MIP-211 at P/P_0 = 0.35 (h).

2.6. Application of MIP-211 for adsorption-driven heat transformation

The stepwise water vapor sorption isotherm of MIP-211, with the step pressure located at P/P_0 = 0.3, indicates this material to be a promising adsorbent candidate for water-adsorption-driven chillers. In this regard, MIP-211 holds a record water uptake capacity (0.6 g_{H2O} g_{MOF}^{-1}, corresponding to a volumetric uptake capacity of 0.48 mL_{H2O} mL_{MOF}^{-1}; the calculated cell density is ρ = 0.811 g. mL^{-1}) among all microporous Al-MOF materials that have been investigated for heat reallocation applications (see Figure 3e, and Table S7). The water uptake of MIP-211 at P/P_0 = 0.3 surpasses by far that of the benchmark CAU-23 (0.37

g g^{-1}), MIL-160 (0.35 g g^{-1}), KMF-1 (0.39 g g^{-1}), CAU-10H (0.30 g g^{-1}), MOF-303 (0.40 g g^{-1}), MIL-53-Fum (0.35 g g^{-1}), MOF-333 (0.38 g g^{-1}) and MIL-53-TDC (0.30 g g^{-1}) (see Figure 3f). The isosteric heat of adsorption was calculated by applying the Clausius-Clapeyron equation to water adsorption isotherms collected at 15, 25, and 35 °C exhibiting step positions at relative pressures of 0.27, 0.29, 0.31, respectively (Figure 3b). The resultant value (Figure 3c & S31) of ~ -48 kJ mol^{-1} is in excellent agreement with the GCMC calculated adsorption enthalpy and the value expected by a simple Dubinin approximation at 25 °C (47.0 kJ mol^{-1}), and is only slightly higher than the evaporation enthalpy of water (40.8 kJ mol^{-1}) due to the high relative pressure at the uptake step. The moderate value of the enthalpy of adsorption suggests that the water adsorbed by MIP-211 could be desorbed with moderate amounts of regeneration heat resulting in higher cycle efficiencies.

The robustness of MIP-211 was finally tested in order to assess its practical usage for thermally-driven adsorption cooling applications. Thermogravimetric analysis (TGA) and variable temperature-depended powder X-ray diffraction (VT-PXRD) revealed that the framework of MIP-211 is thermally stable up to 250 °C, meanwhile, it decomposes at 300 °C. MIL-53-muc is slightly more thermally stable up to 350 °C (see Figure S25 and S26). Noteworthy, MIP-211 maintains its crystalline integrity and porosity over stirring the material for 24 h in acidic (pH 2) and basic (pH = 12) aqueous solutions, as well as in boiling water. Nevertheless, about 14% decrease in the BET surface area and pore volume was observed for the material treated in boiled water (see Figures S27 & 28). Furthermore, multiple water adsorption/desorption cycles were performed with MIP-211, which showed only a slight (< 2%) decrease in the water uptake capacity during the first seven cycles, which remained constant for the rest of the first round of 20 cycles (Figure 3d). Noteworthy, the second round of 20 cycles with the same material did not show any change in the crystallinity, porosity, or water uptake capacity of the material (Figure 3d & S30). All aforementioned hydrothermal, chemical and multicycle water ad-/adsorption stabilities make therefore MIP-211 a highly suitable adsorbent to be applied for adsorption-driven heat transfer.

The possible temperatures (i.e., the desired cooling, back cooling/heat rejection, and driving temperatures) under which MIP-211 can be used for AHT application, and the corresponding efficiencies were determined using the equilibrium water adsorption data (see details in the supporting information).[87] For a typical application requiring a driving temperature of about 10 K, MIP-211 was found to be suitable for adsorption-based cooling with temperature conditions of, e.g., 20 °C, 30 °C and 60 °C (or 25 °C, 35 °C and 65 °C etc.) for cooling, heat rejection to the ambient and driving heat, respectively. This indicates that, the material is perfectly suitable for low-lift applications like moderate cooling of buildings or data centers without dehumidification, but less suitable for high-lift applications like refrigeration or cooling under high ambient temperatures. Obviously, the low-lift characteristic allows exploiting low-grade driving heat sources like waste or

solar heat. Application to large-lift applications, like air conditioning in hot climates or refrigeration will not be possible.

The expected coefficient of performance (COP) was estimated for an adsorption-based cooling application. We assumed, as detailed by Wittstadt,[88] that a fin and tube heat exchanger were coated with 0.1 kg m^{-2} of MIP-211 adsorbent per heat exchanger area. This resulted in a total heat capacity of the heat exchanger per adsorbent mass of 7.7 kJ kg^{-1} K^{-1}. The cooling coefficient of performance (COP) was calculated based on the energy balance of the adsorption heat transformation cycle (see details in the supporting information).[89] The resulting COP values for cooling (Figure 5 top) show a superior performance of MIP-211 for small lifts, where a driving temperature of 60 °C is sufficient to allow for a maximum cooling COP of 0.63. This outperforms all other materials investigated here; especially MIL-53-Fum and CAU-23,[90,62] which both have a similar temperature characteristic. No other material is known with a higher performance under these conditions.

The step in the temperature dependency of the COP is directly related to the step-like isotherm as it depends on the temperature and whether this step can be exploited for the cycle or not. The results also confirm the aforementioned low-lift characteristic, which manifests as a strong sensitivity to the temperature level of the heat rejection T_M (Figure 5b). As soon as T_M exceeds 31 °C (for T_L = 20 °C), the COP decreased dramatically as it does for MIL-53-Fum or CAU-23. For these harsher conditions, more hydrophilic materials like CAU-10H, and lather MIL-160 are required.[91,92] The state-of-the-art silica gel (Siogel®, Oker Chemie) is outperformed by the MOFs under all conditions,[93] and a considerable increase compared to aluminum fumarate (MIL-53-Fum), which is applicable to similar temperature conditions.

It is important to note that the “technically-expectable” approach, used in this work, differs from the “ideal material COP” which is popular in fundamental material literature but where the heat capacity of any heat exchanger structure, driving temperature differences and reduced loading spread are all omitted. Nevertheless, for sake of comparison, we have calculated this COP for different benchmarks. The results (Figure 5 bottom) show an ideal COP of about 0.8 for most of the adsorbents investigated as long as the temperature thrust is large enough (Figure 5c) and the temperature lift is small enough (Figure 5d). However, when compared to the results for the cooling COP, these temperature limits are strongly shifted, suggesting lower driving temperatures and higher heat rejection temperatures because of neglected driving temperature differences. Note, that the conditions investigated here differ from e.g. that used by Lenzen et al (T_L = 10 °C, T_M = 30 °C),[62] as both MIP-211 and CAU-23 have negative cooling COPs under these conditions and only the material COPs suggest a high performance. A detailed comparison is given in the Supplementary Information (Figure S35).

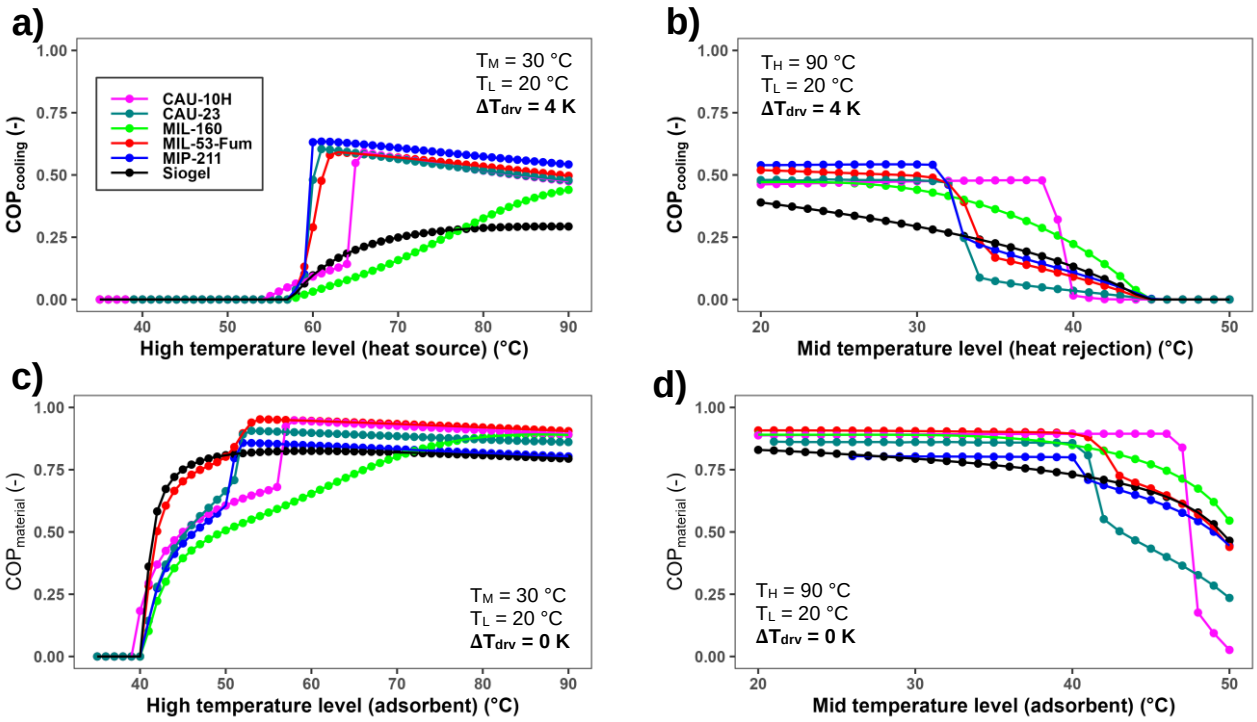

Figure 5. Estimated cooling-COP under typical application conditions (top) and ideal material-COP (bottom) for variations for variations of the high temperature level (left) and the mid temperature level (right) for MIP-211 compared to selected MOFs and a state-of-the-art silica gel (Siogel), showing a superior performance of the novel MIP-211 as long as a low-enough temperature for heat rejection can be provided. Note that for cooling-COPs the temperatures of the exploited heat sink/source differ from the temperatures at material level (driving temperature difference) whereas for material-COPs this difference is neglected resulting in drastic overestimations possible mid temperature levels and underestimation of required high-temperature levels. Negative COPs are set to zero.

2.7. MIP-211 for water harvesting from air. Besides its applicability for ultra-low-temperature-driven cooling, and as a preliminary prospect, we have investigated MIP-211 as a potential candidate adsorbent for sorbent-assisted water harvesting from air. Its combined high uptake capacity, position of the water isotherm at a relative humidity RH = 30 % (P/P_0 = 0.3), multicyclic stability, and low regeneration temperature of MIP-211 (only 60-65 °C) make indeed this material particularly interesting for this application. As a representative showcase, in an arid desert area, the temperature can fluctuate between 38 °C (during the day) and 15 °C (at night), while the relative humidity fluctuates between RH = 10 % (during the day) and RH = 40 % (overnight). The low regeneration temperature of only 65 °C would make it possible to entirely desorb the water from MIP-211 using only solar radiation. In a passive situation, whereby the MIP-211-assisted water harvester operates without any auxiliary energy supply, the working capacity under the aforementioned desert conditions reaches 0.5 L_{H2O} kg_{MOF} day^{-1} (corresponding to a single water adsorption-desorption cycle per day). 4 kg of MIP-211 would still supply 2 L of water, which satisfies the drinkable water demand of an adult. This value surpasses significantly the water deliverable capacity of benchmark MOFs: MOF-801 (0.25 L_{H2O} kg_{MOF} day^{-1}),[94] MOF-160 (0.31–0.33 L_{H2O} kg_{MOF}

day^{-1}),[95] and MOF-303 (0.38 L_{H2O} kg_{MOF} day^{-1})[63] for a single daily cycle. For the evaluation of MIP-211 in a context of active regeneration, whereby the water harvester achieves multiple cycles per day, using active auxiliary systems for heating, transport, and condensation (e. g., driven by solar electricity), the water sorption dynamics of MIP-211 shall still to be determined in further studies.

2.8 Exploratory synthesis optimization

In view of their intended use, the next generation MOFs should also, among other criteria, be synthesized under nontoxic, energy saving and large scalable synthetic routes.[96] For this reason, the sustainable production of MIP-211 in a DMF-free synthesis was tentatively explored using several aluminum sources in water. Interestingly, in a preliminary attempt, MIP-211 was alternatively obtained from the reaction of H_2muc with hydrated aluminum hydroxide ($Al(OH)_3{\cdot}xH_2O$ in water under reflux conditions (see details in the experimental section and Figures S18-S20). Although, this promising protocol still needs to be further optimized to reach pure MIP-211, the MOF could be obtained at the g-scale in a relative short time reaction (6 h).

3. Conclusion

This work demonstrates that not only polymorphism is possible in Al-MOFs with chain-like IBUs, whereby a given aluminum-dicarboxylate MOF could be structural formed with either rod-like chains of *trans*-connected or helical chains of *cis*-connected corner-sharing AlO_6 octahedra, depending on the synthesis conditions employed but is a powerful tool to tune the water sorption properties of MOFs. The *cis*-μ-OH-connectivity results indeed in drastic increase of the hydrophilicity compared to that of the MOF with the *trans*-μ-OH-connectivity, due to the ease of water molecule to preferable bridge between two neighboring μ-OH groups of the IBU, which is more improbable for trans-connected μ-OH groups. The new polymorphism, therefore, induces a strong change in the hydrophilicity of Al-MOFs and the relative pressure position of the step of water sorption isotherm. In the case of the newly discovered hydrothermally stable MIP-211, its water sorption profile and uptake capacity surpass most of the benchmark materials investigated for water sorption applications while exhibiting a very low temperature of regeneration. This concept which is here well exemplified by using *t,t*-muconate is expected to be generalized to other dicarboxylate linkers.

Experimental section

Materials and methods: All chemicals were purchased from Alfa Aesar and used without further purification. $Al_2(SO_4)_3{\cdot}18H_2O$, $Al(OH)_3{\cdot}3H_2O$, $Al(NO_3)_3{\cdot}9H_2O$, $Al(OH)(Ac)_2$, *N,N*'-dimethylformamide (DMF), DMSO.

The initial synthesis of MIP-211: 2.176 g (3.26 mmol) of $Al_2(SO_4)_3{\cdot}18H_2O$ and 0.464 g (3.26 mmol) of *t*,*t*-muconic acid were introduced in a solvent mixture made of 15 mL water and 5 mL DMF. The suspension was heated 6 h while stirring under reflux conditions in a 100 mL round-bottom flask. After cooling to room temperature, the solid product was collected by centrifugation and washed thrice with DMF (10 mL) and thrice with water (10 mL). The product was dried in air after it was activated by heating at 120 °C under a dynamic vacuum for 16 h. 520 mg of material was obtained (92% yield based on H_2muc).

Green synthesis of MIP-211: 5.4 g (41 mmol) of $Al(OH)_3{\cdot}3H_2O$ and 5.8 g (41 mmol) of *t*,*t*-muconic acid were introduced in 500 mL of water and heated 6 h while stirring under reflux conditions in a 1 L round-bottom flask. After cooling to room temperature, the solid product was collected by centrifugation and washed thrice with DMSO (200 mL) and thrice with water (200 mL). . 6.8 g of material was obtained (90% yield based on H_2muc).

Synthesis of MIL-53-muc: 1.2 g (3.2 mmol) of $Al(NO_3)_3{\cdot}9H_2O$ and 0.5 g (3.52 mmol) of *t*,*t*-muconic acid were dissolved in a solvent mixture made of 11.2 mL of water and 3,8 mL DMF. The mixture was sealed in a Teflon-lined autoclave and heated for 6 h at 120 °C in an oven. Once the reactor was cooled down to room temperature, the product was separated and washed as described above. 450 mg of material was obtained (69% yield based on H_2muc).

Powder X-ray diffraction: Routine powder X-ray diffraction (PXRD) data were collected using a high-throughput Bruker D8 Advance diffractometer working on transmission mode and fitted with a focusing Göbel mirror. The X-ray source was Cu-Kα radiation (λ = 1.5418 Å). High-resolution Powder X-ray diffraction (HR-PXRD) data for structure solution was collected with a sample sealed in 0.7 mm glass capillary with a PANalytical EMPYREAN diffractometer (CuKα1 radiation with Ge [1 1 1] monochromator, λ = 1.540598 Å) equipped with a PIXcel1D detector. Temperature-dependent PXRD data were recorded with sample closely packed in quartz capillary on a PANalytical EMPYREAN diffractometer with CuKα radiation (λ = 1.5418 Å) and equipped with an HTK-1200N (Anton Parr) high-temperature chamber and a GaliPIX3D detector.

Elemental analysis (CHN) was performed using a PerkinElmer 2400 series 2 elemental analyzer.

The *Raman* spectra were obtained on a Bruker MultiRAM-FT Raman spectrometer equipped with a Nd: YAG-laser (wavelength 1064 nm). The measurements were executed in the solid state for 2500 scans with a laser power between 10 and 20 mW.

Thermal gravimetric analysis: TGA data were collected on Mettler Toledo TGA/DSC 2, STAR System apparatus with a heating rate of 5 °C/min under the oxygen flow.

Fourier transform Infrared spectroscopy: Infrared spectra were measured with a Nicolet iS5 FTIR ThermoFisher spectrometer.

Scanning electron microscopy (SEM) images were obtained using a JEOL JSM-6510LV QSEM advanced electron microscope with a LaB_6 cathode at 5–20 keV.

Sorption measurement:

Gas sorption: All Nitrogen porosimetry data were collected on a Micromeritics Tristar instrument at 77K. In all the cases the measurements were recorded using ultra-high purity gases (≥4.8 grade). Prior to the adsorption measurement, all the samples were degassed at a certain temperature (180-200°C) for 8 hours. The degassing was done in one step using a Micromeritics SmartVacPrep degas unit: evacuation at 180-200ºC on the degas port ($P=10^{-6}$ mbar), at which point the outgassing rate was ≤ 2 µbar/min.

vapor sorption: The volumetric water sorption measurements were collected using a Micromeritics-triflex instrument. Prior to all the measurements, the sample was degassed using a Micromeritics SmartVacPrep degas unit. The air in the solvent reservoir was removed by freezing the solvent with liquid nitrogen and applying vacuum at the same time. The solvent was then allowed to melt and the process was continued for 2 times to remove all the dissolved gases in the solvent. The temperature during the isotherm measurements was maintained using a chiller unit from Micromeritics.

The multiple cycles adsorption-desorption stability test was carried out with a gravimetric SPS11-10µ water sorption analyzer from proUmid, Germany. About 100 mg of activated (degassed by heating at 120 °C under dynamic vacuum for 16 h) sample was placed in the chamber and the mass change was recorded every 10 min using an electronic balance with an accuracy of ±10 µg as the relative humidity was alternatively varied in the chamber between 0% and 90% at 25 °C under a maximum equilibration time of 3 hours per climate cycle. The experiment was realized for the first run of 20 cycles and then repeated for the second run of 20 cycles without further activation.

Molecular simulations

^{1}H, ^{13}C ^{27}Al NMR parameters were calculated at the DFT level to confirm the line assignment of the MIL-53-muc and MIP-211 structures with the CASTEP code.[97,98] The crystal structures of dry MIL-53-muc and MIP-211 MOFs were initially fully optimized, i.e., both the atomic positions and cell parameters were thoroughly optimized. Grand canonical Monte Carlo (GCMC) simulations were performed to elucidate H_2O adsorption mechanisms of the DFT-optimized crystal structures of MIL-53-muc and MIP-211 MOFs at 298 K using a mixed set of UFF[99] and DREIDING[100] force field parameters and DDEC atomic partial charges of the framework atoms calculated using the CHARGEMOL module.[101,102,103] Water molecules were described by TIP4P/2005 potential model.[104]Full details of these calculations are provided in the supporting information.

Acknowledgements

M. Wahiduzzaman, E. Laurenz, and I. Cornu, contributed equally to this work. The work leading to this publication was supported by the Postdoctoral Researchers Mobility Experience (P.R.I.M.E) program of the German Academic Exchange Service (DAAD) with funds from the German Federal Ministry of Education and Research (BMBF). The computational work was performed using HPC resources from GENCI-CINES (Grant A0120907613).

Conflict of Interest

The authors declare no conflict of interest.

Supporting information

Supporting information is available from the Wiley Online Library or the authors.

References

[1] Y. I. Aristov, *Appl. Therm. Eng*. **2013**, *50*, 1610.

[2] S. K. Henninger, S.-J. Ernst, L. Gordeeva, P. Bendix, D. Fröhlich, A. D. Grekova, L. Bonaccorsi, Y. Aristov, J. Jaenchen, *Renew. Energy* **2017**, *110*, 59.

[3] J. M. Pinheiro, S. Salústio, J. Rocha, A. A. Valente, C. M. Silva, *Renew. Sust. Energ. Rev*. **2020**, *119*, 109528.

[4] P. R. Chauhan, S. C. Kaushik, S. K. Tyagi, *Renew. Sust. Energ. Rev*. **2022**, *154*, 111808.

[5] M. Bilal, M. Sultan, T. Morosuk, W. Den, U. Sajjad, M. M. A. Aslam, M. W. Shahzad, M. Farooq, *Int. Commun. Heat Mass Transf*. **2022**, *133*, 105961.

[6] A. LaPotin, H. Kim, S. R. Rao, E. N. Wang, *Acc. Chem. Res*. **2019**, 52, 1588.

[7] S. K. Henninger, H. A. Habib, C. Janiak*J. Am. Chem. Soc*. **2009**, *131*, 2776.

[8] F. Jeremias, D. Fröhlich, C. Janiak, S. K. Henninger, *New J. Chem*. **2014**, *38*, 1846.

[9] Y. I. Aristov, *Fut. Cit.& Env*. **2015**, *1*, 10.

[10] R. Z. Wang and R. G. Oliveira, *Prog. Energy Combust. Sci*., **2006**, *32*, 424.

[11] N. M. Wajid, A. M. Z. Abidin, M. Hakemzadeh, H. Jarimi, A. Fazlizan, M. F. Fauzan, A. Ibrahim, A. H. A. Al-Waeli, K. Sopian, *Case Studies in Thermal Engineering*, **2021**, *27*, 101275.

[12] M. J. Kalmutzki, C. S. Diercks, O. M. Yaghi, *Adv. Mater.* **2018**, 1704304.

[13] W. Xu, O. M. Yaghi, *ACS Cent. Sci*. **2020**, *6*, 1348.

[14] H. Yang, H. Zhu, M. M. R. M. Hendrix, N. J. H. G. M. Lousberg, G. de With, A.C. C. Esteves, J. H. Xin, *Adv. Mater*. **2013**, *25*, 1150.

[15] F. Fathieh, M. J. Kalmutzki, E. A. Kapustin, P. J. Waller, J. Yang, O. M. Yaghi, *Sci. Adv.* **2018**, *4*, eaat3198.

[16] J. Lord, A. Thomas, N. Treat, M. Forkin, R. Bain, P. Dulac, C. H. Behroozi, T. Mamutov, J. Fongheiser, N. Kobilansky, S. Washburn, C. Truesdell, C. Lee, P. H. Schmaelzle, *Nature* **2021**, *598*, 611.

[17] M. H. Bagheri, S. N. Schiffres, *Langmuir* **2018**, *34*, 1908.

[18] H. Furukawa, F. Gándara, Y.-B. Zhang, J. Jiang, W. L. Queen, M. R. Hudson, O. M. Yaghi, *J. Am. Chem. Soc*. **2014**, *136*, 4369.

[19] N.X. Zhu, Z.-W. Wei, C.-X. Chen, X.-H. Xiong, Y.-Y. Xion, Z. Zeng, W. Wang, J.-J. Jiang, Y.-N. Fan, C.-Y. Xion, Z. Zeng, W. Wang, J.-J. Jiang, Y.-N. Fan, C.-Y. Su, *Angew. Chem. Int.* **2022**, *61*, e202112097.

[20] B. B. Saha, K. Uddin, A. Pal, K. Thu, *JMST Adv*. **2019**, *1*, 161.

[21] H. Lu, W. Shi, Y. Guo, W. Guan, C. Lei, G. Yu, *Adv. Mater*. **2022**, *34*, 2110079.

[22] S.-I. Kim, T.-U. Yoon, M.-B. Kim, S.-J. Lee, Y.K. Hwang, J.-S. Chang, H.-J. Kim, H.-N. Lee, U.-H. Lee, Y.-S. Bae, *Chem. Eng. J.* **2016**, *286*, 467.

[23] F. Trapani, A. Polyzoidis, S. Loebbecke, C. G. Piscopo, *Microporous Mesoporous Mater.* **2016**, *230*, 20.

[24] X. Liu, X. Wang, F. Kapteijn, *Chem. Rev*. **2020**, *120*, 8303.

[25] H. Kim, S. Yang, S. R. Rao, S. Narayanan, E. A. Kapustin, H. Furukawa, A. S. Umans, O. M. Yaghi, E. N. Wang, *Science* **2017**, *356*, 430.

[26] M. F. de Lange, K. J. F. M. Verouden, T. J. H. Vlugt, J. Gascon, F. Kapteijn*Chem. Rev*. **2015**, *115*, 12205.

[27] A. J. Rieth, S. Yang, E. N. Wang, M. Dincă*ACS Cent. Sci*. **2017**, *3*, 668.

[28] D. M. Steinert, S.-J. Ernst, S. K. Henninger, C. Janiak, *Eur. J. Inorg. Chem.* **2020**, *48*, 4502.

[29] S. Cui, M. Qin, A. Marandi, V. Steggles, S. Wang, X. Feng, F. Nouar, C. Serre, *Sci. Rep.* **2018**, *8*, 15284.

[30] H. Furukawa, K. E. Cordova, M. O'Keeffe and O. M. Yaghi, *Science* **2013**, *341*, 1230444.

[31] C. Janiak and J. K. Vieth, MOFs, *New J. Chem*. **2010**, *34*, 2366.

[32] S. T. Meek, J. A. Greathouse, M. D. Allendorf, *Adv. Mater*. **2011**, *23* , 249.

[33] F. Jeremias, V. Lozan, S. K. Henninger, C. Janiak, *Dalton Trans*. **2013**, *42*, 15967.

[34] A. Cadiau, J. S. Lee, D. D. Borges, P. Fabry, T. Devic, M. T. Wharmby, C. Martineau, D. Foucher, F. Taulelle, C.-H. Jun, Y. K. Hwang, N. Stock, M. F. De Lange, F. Kapteijn, J. Gascon, G. Maurin, J.-S. Chang, C. Serre, *Adv. Mater*. **2015**, *27*, 4775.

[35] B. Han, A. Chakraborty, *J. Mol. Liq*. **2021**, *341*, 117381.

[36] K. H. Cho, P. G. M. Mileo, J. S. Lee, U-H. Lee, J. Park, S. J. Sho, S. K. Chitale, G. Maurin, J.-S. Chang, *ACS Appl. Mater. Interfaces* **2021**, 13, 1723.

[37] C. Schlüsener, M. Xhinovci, S.-J. Ernst, A. Schmitz, N. Tannert, C. Janiak, *Chem. Mater*. **2019**, *31*, 4051.

[38] J. Choi, L.-C. Lin, J. C. Grossman, *J. Phys. Chem. C* **2018**, *122*, 5545.

[39] J. Canivet, J. Bonnefoy, C. Daniel, A. Legrand, B. Coasne, D. Farrussen*gNew J. Chem*. **2014**, *38*, 3102.

[40] C. R. Wade, T. Corrales-Sanchez, T. C. Narayan, M. Dincă, *Energy Environ Sci*. **2013**, *6*, 2172.

[41] G. Mouchaham, F. S. Cui, F. Nouar, V. Pimenta, J.-S. Chang, C. Serre, *Trends Chem*. **2020**, *2*, 990.

[42] Z. Zheng, N. Hanikel, H. Lyu, O. M. Yaghi, *J. Am. Chem. Soc*. **2022**, *49*, 22669.

[43] V. Bon, I. Senkovska, I. A. Baburin, S. Kaskel, *Cryst. Growth Des*. **2013**, *13*, 1231.

[44] F. Drache, V. Bon, I. Senkovska, J. Getzschmann, S. Kaskel, *Phil. Trans.R. Soc. A* **2017**, *375*, 20160027.

[45] N. Zhu, M. J. Lennox, T. Düren, W. Schmitt, *Chem. Comm*. **2014**, *50*, 4207.

[46] J.-P. Zhang, X.-Chun Huang, X.-Ming Chen, *Chem. Soc. Rev*. **2009**, *38*, 2385.

[47] T. A. Makal, A. A. Yakovenko, H.-C. Zhou, *J. Phys. Chem. Lett*. **2011**, *2*, 1682.

[48] D. Aulakh, J. R. Varghese, M. Wriedt, *Inorg. Chem*. **2015**, *17*, 8679.

[49] Y. Lo, C. H. Lam, C.-W. Chang, A.-C. Yang, D.-Y. Kang, *RSC Adv*. **2016**, *6*, 89148.

[50] Z.-J. Li, Y. Lu, Z. Zhang, H. Lu, Y. Li, N. Zhang, X.-L. Du, X. Guo, Z.-H. Zhang, Y. Qian, M.-Y. He, *Chem. Eur. J.* **2021**, *27*, 17586.

[51] C. Avendano, Z. Zhang, A. Ota, H. Zhao, K. R. Dunbar, *Angew. Chem. Int. Ed.* **2011**, *50*, 6543.

[52] N. S. Bobbitt, A. S. Rosen, R. Q. Snurr, *Fluid Ph. Equilibria* **2020**, *519*, 112642.

[53] M. Gaab, : Trukhan, S. Maurer, R. Gummaraju, U. Müller, *Microporous Mesoporous Mater*. **2012**, *157*, 131.

[54] T. Wu, N. Prasetya, K. Li, *J. Memb. Sci*. **2020**, *615*, 118493.

[55] F. Jeremias, D. Fröhlich, C. Janiak and S. K. Henninger, *RSC Adv*. **2014**, *4*, 24073.

[56] H. Kummer, F. Jeremias, A. Warlo, G. Füldner, D. Fröhlich, C. Janiak, R. Gläser, S. K. Henninger, *Ind. Eng. Chem. Res*. **2017**, *56*, 8393.

[57] D. Lenzen, P. Bendix, H. Reinsch, D. Fröhlich, H. Kummer, M. Möllers, P. P. C. Hügenell, R. Gläser, S. Henninger, N. Stock, *Adv. Mater.* **2018**, *30*, 1705869.

[58] D. Fröhlich, S. K. Henninger, C. Janiak, *Dalton Trans*. **2014**, *43*, 15300.

[59] D. Fröhlich, E. Pantatosaki, P. D. Kolokathis, K. Markey, H. Reinsch, M. Baumgartner, M. A. Van der Veen, D. E. De Vos, N. Stock, G. K. Papadopoulos, S. K. Henninger, C. Janiak, *J. Mater. Chem. A* **2016**, *4*, 11859.

[60] M. F. De Lange, T. Zeng, T. J. H. Vlugt, J. Gascon, F. Kapteijn, *CrystEngComm* **2015**, *17*, 5911.

[61] N. Tannert, S.-J. Ernst, C. Jansen, H.-J. Bart, S. K. Henninger, C. Janiak, *J. Mater. Chem. A*, **2018**, *6*, 17706.

[62] D. Lenzen, J. Zhao, S.-J. Ernst, M. Wahiduzzaman, A. K. Inge, D. Fröhlich, H. Xu , H.-J. Bart, C. Janiak, S. Henninger, G. Maurin, X. Zou, N. Stock, *Nat. Commun*. **2019**, *10*, 3025.

[63] N. Hanikel, M. S. Prévot, F. Fathieh, E. A. Kapustin, H. Lyu, H. Wang, N. J. Diercks, T. G. Glover, O. M. Yaghi, *ACS Cent. Sci*. **2019**, *5*, 1699.

[64] A. Permyakova, O. Skrylnyk, E. Courbon, M. Affram, S. Wang, U-H. Lee, A. H. Valekar, F. Nouar, G. Mouchaham, T. Devic, G. De Weireld, J.-S. Chang, N. Steunou, M. Frère, C. Serre, *ChemSusChem* **2017**, *10*, 1419.

[65] E. Gkaniatsou, C. Chen, F. S. Cui, X. Zhu, P. Sapin, F. Nouar, C. Boissière, C. N. Markides, J. Hensen, C. Serre, *Cell Rep. Phys. Sci*. **2022**, *3*, 100730.

[66] M. P. Silva, A. M. Ribeiro, C. G. Silva, I. B. R. Nogueira, K.-H. Cho, U.-H. Lee, J. L. Loureiro, J.-S. Chang, A. E. Rodrigues, A. Ferreira, *Adsorption* **2021**, *27*, 213.

[67] K. H. Cho, D. D. Borges, U-H. Lee, J. S. Lee, J. W. Yoon, S. J. Cho, J. Park, W. Lombardo, D. Moon, A. Sapienza, G. Maurin, J.-S. Chang, *Nat. Commun*. **2020**, *11*, 5112.

[68] K. H. Cho, D. D. Borges, J. S. Lee, J. Park, S. J. Cho, D. Jo, U-H. Lee, G. Maurin, J.-S. Chang, *ACS Sustainable Chem. Eng*. **2022**, *10*, 7010.

[69] D. Shade, B. Marszalek, K. S. Walton, *Adsorption* **2021**, *27*, 227.

[70] F. Milange, C. Serre, G. Ferey, *Chem. Commun*. **2002**, 822.

[71] T. Loiseau, C. Serre, C. Huguenard, G. Fink, F. Taulelle, M. Henry, T. Bataille, G. Férey, *Chem. Eur. J*. **2004**, *10*, 1373.

[72] H. Reinsch, M. A. Van der Veen, B. Gil, B. Marszalek, T. Verbiest, D. De Vos, N. Stock, *Chem. Mater.* **2013**, *25*, 17.

[73] H. Reinsch, S. Waitschat, N. Stock, *Dalton Trans*. **2013**, *42*, 4840.

[74] N. Hanikel, x. Pei, S. Chheda, H. Lyu, W. Jeong, J. Sauer, L. Gagliardi, O. M. Yaghi, *Science* **2021**, *374*, 454-459.
[75] T. Rabe, E. S. Grape, H. Rohr, H. Reinsch, S. Wöhlbrandt, A. Lieb, A. K. Inge, N. Stock, *Inorg. Chem*. **2021**, *60*, 8861.

[76] T. J. Matemb Ma Ntep, H. Reinsch, P. P. C. H¨ugenell, S.-J. Ernst, E. Hastürk, C. Janiak, *J. Mater. Chem. A* **2019**, *7*, 24973.

[77] E. Alvarez, N. Guillou, C. Martineau, B. Bueken, B. Van de Voorde, C. Le Guillouzer, P. Fabry, F. Nouar, F. Taulelle, D. de Vos, J.-S. Chang, K. H. Cho, N. Ramsahye, T. Devic, M. Daturi, G. Maurin, C. Serre, *Angew. Chem*. **2015**, *127*, 3735.

[78] A. T.F.Batista, D. Wisser, T. Pigeon, D. Gajan, F. Diehl, M. Rivallan, L. Catita, A.-S. Gay, A. Lesage, C. Chizallet, P. Raybaud, *J. Catal*. **2019**, *378*, 140.

[79] V. Favre-Nicolin, R. Černý, *J. Appl. Cryst*. **2002**. *35*, 734.

[80] J. Rodriguez-Carvajal, *Physica B* **1993**, *192*, 55**.**

[81] M. Wahiduzzaman, D. Lenzen, G. Maurin, N. Stock, M. T. Wharmby, *Eur. J. Inorg. Chem*. **2018**, 3626.

[82] F.-X. Coudert, A. U. Ortiz, V. Haigis, D. Bousquet, A. H. Fuchs, A. Ballandras, G. Weber, I. Bezverkhyy, N. Geoffroy, J.-P. Bellat, G. Ortiz, V. Haigis, J. Patarin, A. Boutin, A. Boutin, *J. Phys. Chem. C* 2014, 118, 10, 5397.

[83] G. Brunner, In *Supercritical Fluid science and Technology*, Vol. 5 (Ed: G. Brunner), Elsevier, *2014*, Ch. 2, pp 9-93.

[84] P. D. Kolokathis, E. Pantatosaki, G. K. Papadopoulos, *J. Phys. Chem. C* **2015**, *119*, 20074.

[85] F. Salles, S. Bourrelly, H. Jobic, T. Devic, V. Guillerm, P. Llewellyn, C. Serre, G. Ferey, G. Maurin, *J. Phys. Chem. C*. **2011**, *115*, 10764.

[86] T. Splith, E. PantatosakiP. D. Kolokathis, D. Fröhlich, K. Zhang, G. Füldner C. Chmelik, J. Jiang, S. K. Henninger, F. stallmach, G. K. Papadopoulos, *J. Phys. Chem. C* **2017**, *121*, 18065.

[87] E. Laurenz, *Doctoral thesis*, Technische Universität Hamburg **2021**.

[88] U. Wittstadt, *Doctoral dissertation*, Technische Universität Berlin **2018**.

[89] L. Schnabel, G. Füldner, A. Velte, E. Laurenz, P. Bendix, H. Kummer, U. Wittstadt, In *Innovative Heat Exchangers* (eds: by H.-J. Bart, S. Scholl), Springer International Publishing **2018**, pp. 363-394.

[90] E. Laurenz, G. Füldner, L Schnabel, G. Schmitz, *Energies* **2020**, *13*, 3003.

[91] S.-J. Ernst, M. Baumgartner, D. Fröhlich, H.-J. Bart, S. K. Henninger, *Chem. Eng. Tech.* **2017**, *89*, 1650.

[92] S. Gökpinar, S.-J. Ernst, E. Hastürk, M. Möllers, I, ElAita, R. Wiedey, N. Tannert, S. Nießing, S. Abdpour, J. Quodbach, G. Füldner, S. K. Henninger, C. Janiak, *Ind. Eng. Chem. Res.* **2019**, 58, 47, 21493.

[93] A. Sapienza, A. Velte, I. Girnik, A. Frazzica, G. Füldner, L. Schnabel, Y. Aristov, *Renew. Energy* **2017***, 110***,** 40.

[94] H. Kim, S. R. Rao, E. A. Kapustin, L. Zhao, S. Yang, O. M. Yaghi, E. N. Wang, *Nat. Commun*. **2018**, *9*, 1191.

[95] M. Solovyeva, I. Krivosheeva, L. Gordeeva, Y. Aristov, *Energies* **2021**, *14*, 3586.

[96] M. I. Severino, E. Gkaniatsou, F. Nouar, M. L. Pinto, C. Serre, *Faraday Discuss.* **2021**, *231*, 326.

[97] M. D. Segall, P. J. D. Lindan, M. J. Probert, C. J. Pickard, P. J. Hasnip, S. J. Clark, M. C: Payne, *J. Phys.: Condens. Matter* **2002**, *14*, 2717.

[98] S. J. Clark, M. D. segall, C. J. Pickard, P. J. Hasnip, M. I. J. Probert, K. Refson, M. C. Payne, *Z. Kristallogr*. **2005**, *220*, 567.

[99] A. K. Rappe, C. J. Casewit, K. S. Colwell, W. A. Goddard, W. M. Skiff, *J. Am. Chem. Soc*, **1992**, *114*, 10024.

[100] S. L. Mayo, B. D. Olafson, W. A. Goddard, *J. Phys. Chem*. **1990**, *94*, 8897.

[101] N. G. Limas, T. A. Manz, *RSc Adv*. **2016**, 45727.

[102] T. A. Manz, *RSC Adv*. **2017**, *7*, 45552.

[103] N. G. Limas, T. A. Manz, *RSC Adv*. **2018**, *8*, 2678.

[104] J. L. F. Abascal, C. Vega, *J. Chem. Phys*. **2005**, *123*, 234505.